Research Repository UCD

Title	Damage detection and calibration from beam–moving oscillator interaction employing surface roughness
Authors(s)	Jaksic, Vesna, O'Connor, Alan, Pakrashi, Vikram
Publication date	2014-08-18
Publication information	Jaksic, Vesna, Alan O'Connor, and Vikram Pakrashi. "Damage Detection and Calibration from Beam–moving Oscillator Interaction Employing Surface Roughness" 333, no. 17 (August 18, 2014).
Item record/more information	http://hdl.handle.net/10197/10404
Publisher's statement	This is the author's version of a work that was accepted for publication in Journal of Sound and Vibration. Changes resulting from the publishing process, such as peer review, editing, corrections, structural formatting, and other quality control mechanisms may not be reflected in this document. Changes may have been made to this work since it was submitted for publication. A definitive version was subsequently published in Journal of Sound and Vibration (333, 17, (2014)) https://doi.org/10.1016/j.jsv.2014.04.009
Publisher's version (DOI)	10.1016/j.jsv.2014.04.009

Downloaded 2024-06-16 02:50:30

The UCD community has made this article openly available. Please share how this access benefits you. Your story matters! (@ucd_oa)

© Some rights reserved. For more information

Damage Detection and Calibration from Beam-Moving Oscillator Interaction Employing Surface Roughness

V. Jaksic[1], A. O' Connor[2] and V. Pakrashi[1]

[1]Dynamical Systems and Risk Laboratory, Department of Civil and Environmental Engineering, University College Cork, Ireland

[2]Department of Civil, Structural and Environmental Engineering, Trinity College Dublin, Ireland

Corresponding Author: Dr. Vikram Pakrashi, Lecturer in Structural Engineering, Department of Civil and Environmental Engineering, University College Cork, Ireland. Phone: +353(0)214903862 Email: V.Pakrashi@ucc.ie Fax: +353(0)214276648

Abstract

The possibility of employing bridge deck surface roughness for Structural Health Monitoring (SHM) under operational conditions is proposed in this paper. A bilinear breathing crack in a damaged Euler Bernoulli beam traversed by a moving oscillator is considered in this regard. The Road Surface Roughness (RSR) of the beam is classified as per ISO 8606:1995(E). The interaction of the moving oscillator with surface roughness is exploited to define simple, consistent, easy to implement and robust statistical descriptors to detect and calibrate the existence, the location and the extent of damage. The effects of vehicle speed and variable RSR profiles for such detection are investigated and preferable conditions for detection are identified. The proposed method is also

suitable for experimental analysis where a theoretical model is not available or is not credibly ascertained.

Keywords: Structural Health Monitoring (SHM), Euler – Bernoulli Beam, Breathing Crack, Road Surface Roughness, Bridge-Vehicle Interaction.

Authors:

Vesna Jaksic, Doctoral Researcher, Department of Civil and Environmental Engineering, University College Cork, Ireland. V.Jaksic@umail.ucc.ie

Dr. Alan O'Connor, Associate Professor in Structural and Environmental Engineering, School of Engineering, Trinity College Dublin, Ireland. alan.oconnor@tcd.ie

1. Introduction

Structural Health Monitoring (SHM) can be a practical tool for remote monitoring of in-service structures aiming to improve the prediction of safety level and system performance while reducing maintenance costs. SHM is also critical for the prioritization of the time and nature of investment in a structure or a network of structures [1-3]. Non-destructive structural damage detection as an essential part of SHM is becoming an important aspect of integrity assessment for aging, inaccessible or extreme-event affected structures. Generally, damages or alterations to a structure tend to change its dynamic characteristics. Often, such damages are local and significant changes are not reflected in the global dynamic response. Consequently, methodologies are developed to capture the local change through some marker to estimate the presence, the location, and the severity of damage. In this regard damage detection employing bridge-vehicle interaction is of considerable interest since the structure can be kept in operation throughout the process.

The problem of bridge-vehicle interaction is well understood [4-6] and there exists a number of numerical methods [7-9] for damage detection. This provides a motivation to employ bridge-vehicle interaction for monitoring damage evolution. Local damages like cracks pose a particular challenge in this respect since the changes are local. The local changes may be attributed to a sharply changing function corresponding to locally appearing high frequency components. With rapidly improving experimental capabilities, the measurement options have also increased to a very significant extent and the implementation of novel methodologies have become more feasible than ever before.

Vibration based techniques for crack detection have been widely employed since they offer fast and inexpensive means for crack identification [10]. Narkis [11] has proposed a method for calculation of natural frequencies of a cracked simply supported beam where the crack is simulated by an equivalent rotational spring. This method was applied to identify crack location from frequency measurements. Recently, there have been works involving bridge-vehicle interaction to detect damage. Law and Zhu [12] have investigated the dynamic behavior of damaged reinforced concrete bridges under moving loads using a model of a simply supported beam with open and breathing cracks. The phase space of the damaged beam response was distorted in comparison with an undamaged phase space. Majumdar and Manohar [13] have proposed time domain damage descriptors to reflect the changes in bridge behavior due to damage represented by local reduction in stiffness. Lee et al. [14] have experimentally investigated the possible application of bridge–vehicle interaction data for identifying the loss of bending rigidity by continuously monitoring the operational modal parameters. Bilello et al. [15] have observed dynamic response of the small-scale bridge model and compared findings

with the continuous Euler–Bernoulli beam theory. Bilello and Bergman [16] have considered, theoretically and experimentally, the response of a damaged Euler–Bernoulli beam traversed by a moving mass, where the damage was modeled through rotational springs. An increase in structural damage sensitivity under the effect of a moving load was observed in this case. Pakrashi et al. [17] have performed experimental investigation of simply supported beam traversed by a moving load and subjected to different levels of damage. The wavelet transformed phase spaces for damaged and undamaged cases differed distinctly at high scales but were often masked due to the presence of noise within the signal. The masking effect has also been observed from a different context by Gentile and Messina [7]. Bu et al. [18] have proposed a damage assessment approach from the dynamic response of a passing vehicle through a damage index and have considered effects of different vehicle models, vehicle speed, vehicle and bridge mass and stiffness ratios, sampling frequency, road surface roughness, measurement noise, and model error. The road surface roughness was observed to affect the bridge-vehicle system similar to a random noise excitation. The maximum dynamic responses were related to the worst surface roughness. Abdel-Rohman and Al-Duaij [19] have recognized the importance of unevenness in the bridge deck on the dynamic response of single span bridges due to moving loads. They have assumed unevenness to be a sinusoidal wave shape function and found that it has a significant effect on the acceleration response. Da Silva [20] has proposed a methodology to evaluate the dynamical effects, displacement and stress on highway bridge decks due to vehicles crossing rough pavement surfaces defined by a probabilistic model. It was concluded that the effects due to interaction of the vehicles with an irregular pavement surface could be more important than those

produced by the load mobility alone. Also, dynamical effects increase drastically with the decrease of pavement surface quality. A lower quality pavement surface was one with an amplitude of irregularity larger than 1.4 cm. Wu and Law [21] have proposed a stochastic vehicle axle load identification algorithm and studied the effect of different road surface profiles on algorithm accuracy. They demonstrated that the Gaussian assumption of the road surface roughness can be helpful.

Although there are many interesting numerical and statistical markers and methods available for damage detection [9, 22-24], surface roughness has always been treated for parameter studies, improved analysis or for establishing the bounds of efficiency of an algorithm. This paper directly uses surface roughness as a main aid to detect damage by focusing only at the high frequency components. Jaksic et al. [25] have investigated the basis of using surface roughness where a white noise excitation response of a single degree of freedom bilinear oscillator was investigated. The white noise represented a broadband excitation, qualitatively similar to the interaction with surface roughness, the bilinearity attempted to capture a breathing crack. The stiffness of one of the springs was theoretically degraded at different levels. It was observed that there are markers [26], i.e. first and second order cumulants of the response of this system in this case, which behave consistently with this change. The conclusions of this work provided an impetus to carry out a damaged-beam vehicle interaction based damage detection study from multiple point observations in the time domain using the interaction with realistic surface roughness, which is presented here. The damage has been modeled as a localized breathing crack and surface roughness has been defined by ISO 8606:1995 [27]. The responses of the first mode of undamaged and damaged beam are observed [9, 28] since

they are easy to detect and are a good approximation of the actual displacement. Cumulant based statistical markers are established for damage detection utilising these responses, using a new detection method. The markers are investigated against key variables like the location and the extent of the crack, vehicle velocity and type of surface roughness in order to obtain preferable conditions of detection. The proposed method is well-suited for output-only operational conditions of bridges and can contribute to the SHM of bridge structures to a significant extent.

2. Theory

The schematic of the problem considered is presented in Figure 1 where the damaged bridge-vehicle interaction system is represented as a simply supported Euler-Bernoulli beam with a breathing crack traversed by a single degree of freedom oscillator. The beam represents the bridge and the oscillator represents the vehicle. The vehicle is assumed to be moving on the surface without losing contact with it. The length of the beam is L (m) and the crack is at a distance x_c (m) from the left support. The beam has a constant cross-sectional area A (m^2) and a second moment of area I (m^4). The material properties of the beam are the Young's modulus E (N/m^2) and the mass density ρ (kg/m^3). The crack is modeled as a rotational spring [11] when the crack is open.

2.1 Equations of motion of a simply supported beam with breathing crack

The governing equation of motion of cracked beam with mass per unit length $m=\rho A$ (kg/m) and structural damping of the material c, subject to the weight of the moving load P (N) are coupled through continuity and jump conditions at crack location as:

$$EI\frac{\partial^4 y_i(x,t)}{\partial x^4} + c\frac{\partial y_i(x,t)}{\partial t} + \rho A\frac{\partial^2 y_i(x,t)}{\partial t^2} = P\delta(x-\upsilon t); \quad i = 1,2 \tag{1}$$

where EI is flexural rigidity (Nm^2); t is the time coordinate with the origin at the instant of the force arriving upon the beam (s); x is the length coordinate with the origin at the simply supported end of each beam (m); $y_i(x,t)$ is the transverse deflection of the i^{th} beam segment at the point x and time t, measured from the static equilibrium position corresponding to when the beam is loaded under its own weight; δ is the Dirac Delta function [25]; and υt is the position of the vehicle moving with constant speed υ from left support (m).The external force P is defined as in [19]:

$$P = \{m_V g + K[z - y_i(\upsilon t, t) - r(\upsilon t)]\}; \quad i = 1,2 \tag{2}$$

where m_V is the mass of the vehicle (kg); g is acceleration due to gravity (9.81 m/s^2); K is the stiffness of the vehicle's tires and springs (N/m); z is the vertical displacement of the vehicle with respect to its static equilibrium position (m);and r is the surface roughness (m). The effects of structural damping are often small [26] and under such circumstances equation (1) can be rewritten as:

$$EI\frac{\partial^4 y_i(x,t)}{\partial x^4} + \rho A\frac{\partial^2 y_i(x,t)}{\partial t^2} = \{m_V g + K[z - y_i(\upsilon t, t) - r(\upsilon t)]\}\delta(x-\upsilon t); \quad i = 1,2 \tag{3}$$

with the condition:

$$K[z - y_i(\upsilon t, t) - r(\upsilon t)] \geq 0 \tag{4}$$

The solution of the eigenvalue problem related to this system provides the natural frequencies and mode shapes. The open and the closed crack states are considered to obtain two sets of natural frequencies and mode shapes for a breathing crack formulation.

2.2 The open crack eigenvalue problem

When the crack is open, the system is considered to consist of two beams connected by a rotational spring, where each continuous segment of the beam can be described by the Bernoulli-Euler partial differential equation of motion (3). The eigenvalue problem can then be solved through the method of separation of variables:

$$y_i(x,t) = \sum_{j=1}^{n} \phi_j^i(x)\, q_j(t); \quad i = 1,2 \tag{5}$$

where ϕ_j^i is the orthogonal mode shape of the i^{th} beam for the j^{th} mode shape and q_j is the time dependent amplitude. By separating temporal and spatial variables, the following differential equation system is obtained:

$$\phi_j^{i\,''''}(x) - \frac{{\omega_j}^2 \rho A}{EI}\phi_j^i(x) = 0\,; \quad i = 1,2; j = 1\ to\ n \tag{6}$$

$$\ddot{q}_j(t) + {\omega_j}^2 q_j(t) = 0; \quad j = 1\ to\ n \tag{7}$$

where ω_j is natural frequency of the beam and the superscripted primes denote differentiation with respect to the spatial coordinate. For free vibrations of the beam, there is no external excitation and consequently there are no displacements or moments at the supports. The corresponding boundary conditions are:

$$x = 0 \implies \phi_j^i(0) = 0; \quad \phi_j^{i\,''}(0) = 0\,; \quad i = 1,2; \ j = 1\ to\ n \tag{8}$$

Boundary conditions at the crack location x_c must satisfy continuity of displacement, bending moment and shear, leading to:

$$\phi_j^1(x = x_c) = \phi_j^2(x = L - x_c) \tag{9}$$

$$\phi_j^{1''}(x = x_c) = \phi_j^{2''}(x = L - x_c) \tag{10}$$

$$\phi_j^{1'''}(x = x_c) = -\phi_j^{2'''}(x = L - x_c) \tag{11}$$

The slope between the two beam segments can be related to the moment at this section as:

$$\phi_j^{1''}(x_c) + \frac{K_T}{EI}\left[\phi_j^{2'}(x = L - x_c) + \phi_j^{1'}(x = x_c)\right] = 0 \tag{12}$$

where K_T is the equivalent rotational spring stiffness as defined by Sundermeyer and Weaver [29] and expressed as a polynomial function of Crack Depth Ratio (CDR). The solution of the spatial differential equation (6) satisfying all eight boundary conditions is thus:

$$0 < \bar{x} < x_c \rightarrow \phi = A(\sin a\bar{x} + \alpha \sinh a\bar{x}) \tag{13}$$

$$x_c < \bar{x} < L \rightarrow \phi = A\left(\frac{\sin(ax_c)\sin\left(a(L-\bar{x})\right)}{\sin\left(a(L-x_c)\right)} + \alpha\frac{\sinh(ax_c)\sinh\left(a(L-\bar{x})\right)}{\sinh\left(a(L-x_c)\right)}\right) \tag{14}$$

where

$$a^4 = \frac{{\omega_j}^2\rho A}{EI} \tag{15}$$

$$\alpha = \frac{\cos ax_c + \dfrac{\sin ax_c}{\tan a(L-x_c)}}{\cosh ax_c + \dfrac{\sinh ax_c}{\tanh a(L-x_c)}} \tag{16}$$

with the constant A chosen so that the mode shapes are normalized as:

$$\int_0^{x_c} (\phi_j(\bar{x}))^2 d\bar{x} + \int_{x_c}^{L} (\phi_j(\bar{x}))^2 d\bar{x} = 1 \quad (17)$$

where the spatial coordinate $\bar{x}$ is considered from the left hand support and ϕ is the generalised representation of any mode shape as $\{\phi_j^1, \phi_j^2\}$ for any mode, arbitrarily represented as the j^{th} mode here.

The natural frequencies of the beam with the open crack can also be calculated replacing boundary conditions in an assumed solution of mode shape equation (6):

$$\phi(x) = A_1 \cos ax + A_2 \sin ax + A_3 \cosh ax + A_4 \sinh ax \quad (18)$$

and setting its determinant to zero, or by using equations (15) and (16) [29]. A comparison of natural frequency results using the approach of Sundermeyer and Weaver [29] was carried out against the approach of Narkis [11] and the results were found to be in agreement.

2.3 The closed crack eigenvalue problem

When the crack closes, the beam is treated as one continuous Euler-Bernoulli beam and the first mode shape equation is:

$$0 < x < L \rightarrow \phi(x) = \sqrt{\frac{2}{L}} sin(ax) \quad (19)$$

Since the displacement at the supports equals zero, the equation (18) is satisfied when *sin (aL)=0*. Therefore the natural frequencies of the beam when the crack is closed are:

$$\omega_j = j^2\pi^2 \sqrt{\frac{EI}{mL^4}}; \quad j = 1, 2, 3, \ldots \quad (20)$$

2.4 Equation of motion of vehicle

The equation of motion of the vehicle, modeled as a single degree of freedom oscillator can be represented as:

$$m_V\ddot{z} + c_V\dot{z} + K[z - r(vt) - y_i(vt, t)] = 0, \qquad i = 1, 2 \tag{21}$$

where c_V is the vehicle damping coefficient.

2.5 Surface roughness

The moving vehicle loads are time dependent, because the position of wheel loads changes with time (t) and the suspension of the vehicle oscillates (z) due to irregularities of the Road Surface Roughness (RSR) [21]. The randomness of the RSR can be represented through a periodic modulated random process [20, 21, 30, 31]. In the ISO 8606:1995(E) [27] specifications, RSR is related to the vehicle's speed by a formula linking velocity and displacement power spectral density (PSD), where the general form of displacement PSD of RSR in (m^3/cycles) is:

$$S_d(f) = S_d(f_0)\left(\frac{f}{f_0}\right)^{-\alpha} \tag{22}$$

where $f_0 = 1/2\pi$ (cycles/m) is the discontinuity frequency; f is the spatial frequency (cycles/m); $S_d(f_0)$ is roughness coefficient (m^3/cycles); α is an exponent of PSD. In this paper, since this roughness classification is based on constant vehicle speed PSD, $\alpha = 2$.

The RSR function $r(\hat{x})$ in its discrete form [21, 30, 31]:

$$r(\hat{x}) = \sum_{k=1}^{N} \sqrt{4S_d(f_0)\left(\frac{2\pi k}{L_c f_0}\right)^{-2}\frac{2\pi}{L_c}}\cos\left(\frac{2\pi k f_0}{L_c} + \theta_k\right) \tag{23}$$

where $\hat{x}$ is the discrete representation of the spatial coordinate.

Here L_c is twice the length of the bridge; N is number of data points of successive ordinates of the surface profile; and θ_k is a set of independent random phase angles uniformly distributed between 0 and 2π.

The road classification according to ISO 8606:1995(E) is based on the value of $S_d(f_0)$ and in this paper five classes of road surface roughness representing different qualities of the road surface have been observed, defined as A-E [18] from the best to the worst respectively, as shown in Table 1.

2.6 Damaged Beam – Moving Oscillator Interaction Including Surface Roughness

The bridge vehicle interaction can be defined by a system of second order differential equations coupling the equations of motion of the beam (1) and of the vehicle (21). For the first mode shape, equations (1) and (21) can be written in matrix form as:

$$\begin{bmatrix} 1 & 0 \\ 0 & 1 \end{bmatrix} \times \begin{Bmatrix} \ddot{q}_1 \\ \ddot{z} \end{Bmatrix} + \begin{bmatrix} 2\xi_1\omega_1 & 0 \\ 0 & 2\xi_V\omega_V \end{bmatrix} \times \begin{Bmatrix} \dot{q}_1 \\ \dot{z} \end{Bmatrix}$$

$$+ \begin{bmatrix} \omega_1^2 + \dfrac{K}{\rho A}\phi_1(vt)\phi_1(vt) & -\dfrac{K}{\rho A}\phi_1(vt) \\ -\omega_V^2\phi_1(vt) & \omega_V^2 \end{bmatrix} \times \begin{Bmatrix} q_1 \\ z \end{Bmatrix}$$

$$= \begin{Bmatrix} \dfrac{m_V g}{\rho A}\phi_1(vt) - \dfrac{K}{\rho A}r(vt)\phi_1(vt) \\ \omega_V^2 r(vt) \end{Bmatrix} \tag{24}$$

where the natural frequency of the vehicle is $\omega_V^2 = \frac{K}{m_V}$; and ξ_j and ξv are the damping ratios of the j^{th} mode of the bridge and that of the vehicle respectively.

The displacements and the velocities of the beam and the vehicle are obtained by solving the system of second order differential equations (24) using a 4/5th order Runge-Kutta method available in Matlab [32].

3. Damage Detection through Surface Roughness

The dynamic response of the beam due to beam-moving oscillator interaction is utilized to detect and calibrate the location and the extent of damage. The data used for the bridge model are, L = 15m; ξ_1 = 2%; E = 200e9N/m^2 and ρ = 7900kg/m^3. The static deflection of the beam is 0.005m. The depth (h) of the beam is 1.5 times the width (b) of the beam. Other geometric descriptors like I, A and other values are computed based on this assumption. For the simulations, the selected values are I = 0.0021m^4 and A = 0.1287m^2. The data used for vehicle are m_v = 3000kg and K = 3.65e6N/m [33]. Responses of the beam and the vehicle corresponding to changes in x_c at mid-span, quarter-span, and close to the support; CDR from small (0.1) to large (0.45) with 0.05 increment; V_v from slow to fast within a range of 10 to 150 km/h with 10 km/h increment and RSR from very good to very poor were considered.

The proposed detection scheme in this paper is illustrated in Figure 2 through an example. The general schematic of the methodology is presented in Figure 3. The beam is first divided into a number of equal segments. In this regard different numbers of segments have been tested. A beam with a minimum of 20 (0.75m) or more reasonably, 100 (0.15m) segments were observed to be adequate for analysis and discussion of the proposed technique based on comprehensive numerical experiments. Figure 2a shows 20 segments. The first mode shape of the beam closed and open crack conditions are computed next. In

Figure 2b the crack is located at mid-span (x_c = 0.5L). The first mode shape differs very little from the undamaged shape from the global point of view. Locally, there exists a discontinuity in the slope of damaged mode shape at the location of damage. The extent of this change of slope, though difficult to detect, is indicative of the extent of damage, since small cracks have little effect on natural frequencies and mode shapes of beams. Only crack ratios larger than 0.5 result in moderate frequency and large mode shape changes [34]. This ratio range is not useful as structure failure will probably occur before such damage extents are reached. The difference between the damaged and the undamaged mode shapes is found (Figure 2c) along with their ordinate values at the middle of each segment. The mode shape difference function ($\Delta\Phi$) has a local maximum and discontinuous slope at the indicated single damage location, although the same will appear in the case of multiple cracks [28]. In the case where cracks are very close to each other, there could be an overlap as these cracks influence each other structurally. In practice, the mode shape difference in the spatial domain may be hard to detect. However, an initial benchmarked estimate of the undamaged mode shape and natural frequency should be carried out even under such circumstances. The bridge response (displacement is chosen in this case) obtained by solving equation (24) is multiplied with the mode shape difference function ordinate at the middle of each segment ($\Delta\Phi_m$) (Figure 2d). The multiplication, $\Delta\Phi_m q(t)$, is not implicit but explicit as in reality the bridge responses are not too difficult to measure using small sensors placed in multiple locations along the structure. The location and the extent of damage is then computed by choosing an appropriate descriptor on the values of $\Delta\Phi_m q(t)$ at multiple locations. The involvement of surface roughness ensures that the high frequency components take part in forming the

descriptor features apart from the slow moving, vehicular weight driven response. This participation cannot be described without the consideration of surface roughness or by representing the vehicle as a moving point load. Noise is cancelled out by considering the passage of many vehicles and the consideration of normalisation. The undamaged mode shape response can be found by considering the estimated values, as mentioned in the previous section. It is observed that the location near the damage is affected in this differenced time domain response (Figure 2d). Figure 3 indicates the steps to reach the multi-point observation signal $\Delta\Phi_m q(t)$, for which an appropriate descriptor of damage is to be chosen. As discussed, the level of participation for each of these elements in the schematic depends on the available information, degree of experimentation and modeling complexity. The location of the damage(s) could be indicated by using wavelet analysis as shown in many papers [9, 35-37]. The presence of multiple damages will be accumulated and represented as a single equivalent damage when considering such an approach if they are too close spatially, correctly indicating that in effect such close damages behave like a single damage of a modified extent. Time-frequency techniques, like wavelet analysis [7, 9] can detect singularities in a signal or sharp local changes in the signal. However, they may require significant computational time for deployment consequently, there remains the interest in developing simple and consistent descriptors from the output so that computation time is minimized when deployed in real time as in SHM system Network.

4. Choice of Damage Detection and Calibration Markers

Statistical descriptors on $\Delta\Phi_m q(t)$ for each segment of the observed beam and for each combination of variables; x_c, CDR, V_v and RSR were investigated for monotonocity and consistency. The statistical measures considered included mean (μ), standard deviation (σ), skewness (λ), and kurtosis (κ). The choice of mean and standard deviation stemmed out of the recent study [25]. In a separate study [23], the skewness and kurtosis were observed to be markers for beam with an open crack vibrating under white noise and consequently these two parameters were also chosen owing to the similarity of the present problem. The parameters are computed as follows:

$$\mu = \frac{1}{m}\sum_{i=1}^{m} x_i \tag{25}$$

$$\sigma = \sqrt{\frac{1}{m}\sum_{i=1}^{m}(x_i - \mu)^2} \tag{26}$$

$$\lambda = \frac{\frac{1}{m}\sum_{i=1}^{m}(x_i - \mu)^3}{\left(\sqrt{\frac{1}{m}\sum_{i=1}^{m}(x_i - \mu)^2}\right)^3} \tag{27}$$

$$\kappa = \frac{\frac{1}{m}\sum_{i=1}^{m}(x_i - \mu)^4}{\left(\frac{1}{m}\sum_{i=1}^{m}(x_i - \mu)^2\right)^2} \tag{28}$$

Additionally, the applicability of a simple R/S analysis based Hurst exponent (H) was also investigated [38] in these studies since this measure has been applied before for predicting events [39, 40] or sudden stiffness changes [41].

Figure 4 shows an example of mean (4a), standard deviation (4b), kurtosis (4c), skewness (4d) and Hurst exponent (4e) measures of $\Delta\Phi_m q(t)$ calculated for each beam segment where crack location is at 0.1L (1.5m) from the left support; 0.25L (3.75m) from the left support and at 0.5L (7.5m) respectively, the vehicle speed is 80km/h, CDR is 0.45 and RSR is class C. It is found that the obtained mean (Figure 4a) and standard deviation (Figure 4b) functions are similar in shape and clearly show the discontinuous slope at the damage location, as per the mode shape difference functions. This finding is consistent with [25] where it has been proven that first and second order cumulants of bilinear and linear system responses are consistent and monotonic descriptors of the system characteristics and are sensitive to sudden changes in stiffness, which can be associated with the sudden failure of a part of a structure. Due to the similarity of the shapes of damage calibration curves related to mean and standard deviation, a Coefficient of Variation (CoV) based marker will not be efficient. This marker was investigated in this study and was confirmed not to be consistent. Following the method proposed by Cacciola et.al [23] for beam vibrating under white noise, kurtosis (Figure 4c) and skewness (Figure 4d) measures were tested but they appear to be insensitive to crack presence for practical ranges of values. Only for the crack located at mid-span, in the proximity of the crack, does the skewness function suddenly change sign, but this change does not have a consistent monotonic trend in case of change of any observed variables. The relative insensitivity of skewness and kurtosis for this detection scheme comes from

the scaling of data of these measures for time domain responses of different segments multiplied by the ordinate of the mode shape difference estimate at the centre of each segment. Hurst exponent (Figure 4e) is also found to be insensitive to presence of the crack. Therefore μ and σ are chosen as markers for further calibration analysis.

5. Results

Figure 5 represents an example of mean and standard deviation functions for the case where the crack is located at quarter-span, RSR is type C, the vehicle is moving with a speed 80km/h and CDR increases from 0.1 to 0.45. From this and the similar figures obtained by varying x_c, RSR type and V_V, a number of observations are noted. The markers μ and σ show slope discontinuity at the damage location. The values of statistical parameters relative to each other increase with increasing CDR and the slope discontinuity of μ and σ at the crack location become more obvious when CDR increases. These indicate that the location of crack can be identified by the chosen markers and that consistent calibration is possible. Values of μ and σ at crack locations for all combinations of x_c, RSR type, CDR, and V_v were investigated. More than 1800 cases were observed in order to establish the calibrations of μ and σ at crack locations and variable dependence of the calibrations. Only the essential findings are presented here. In general, the relation between μ and σ and CDR for different V_V increases exponentially. These curves can be separated into four groups depending on V_V: very low speed (10km/h); low speed (20-60km/h); medium speed (70-100km/h) and high speed (110-150km/h), for which variation of μ and σ is very high, high, medium, and low, respectively. This grouping becomes more obvious for higher CDR when RSR is type D

and E, while for the RSR type A and B there is very little difference between statistical parameters even for a higher values of CDR. The exception is very low V_V for which statistical parameters are observed to be much higher than for other V_V for all cases of RSR. RSR type C and V_V = 80km/h are found to be optimal for calibration purposes.

Figures 6 a) and b) show the relation of μ and σ, respectively with changes in CDR for different positions of the crack along the beam. In general, calibrations are monotonic (μ and σ increase with CDR) but there is no obvious relation between the curves representing different crack locations. This leads to a conclusion that it is not necessarily true that the edge crack has the smallest statistical parameters. Therefore, plotting μ and σ at crack location as a function of crack distance from the left support of the beam for different CDR is more appropriate. This is shown Figures 6 c) and d). It is observed that the values of statistical parameters increase as the position of the crack moves from the support towards the quarter-span (x_c = 0.25L), where it reaches the maximum, and then decrease from quarter-span to 0.4L, to the minimum, before increasing again at mid-span. It is also shown here that more intense cracks are always more responsive in terms of their markers. Since the location of the crack will be identified beforehand, as presented in Figure 5, the calibration of the damage extent can always be projected to specific curves.

The relationship between the statistical parameters and CDR in relation to RSR types for three different V_V (50; 100 and 150km/h representing low, medium and high vehicle speed respectively) are shown in Figure 7. From this figure, it is observed that the statistical descriptors are larger for lower V_V. This becomes more obvious as CDR increases. For RSR type D and E, the variations of μ and σ are more obvious even for

lower vehicle speed, while for type A, B and C it is almost the same for the higher speeds of the vehicle. Therefore the consistency of calibration is dependent on the speed and road type. This is more pronounced when the damage extent is higher. Better roads give consistent but less sensitive results, while worse roads are less consistent in value but give more sensitive results. Therefore, for calibration purposes it is recommended to use RSR type C as an optimum.

Figure 8 shows the results of calibration of standard deviation as a function of vehicle speed variation (low, medium, and high) observed for the position of damage close to the support, at quarter-span and mid-span of the beam. The calibration functions are shown for small, medium, and high CDR. The dotted grey lines represents a 6^{th} degree polynomial fit (which for the coefficients with 95% confidence bounds give the goodness of fit measure of R^2 as 0.9735 and 0.9865, for the worst and the best fit function respectively) which incorporates very low vehicle speeds. A speed of 10km/h shows much higher values of statistical descriptor when compared with other speeds. When the 10km/h value is excluded from the analysis, linear polynomial equations are obtained and represented with the solid line. Corresponding straight line equations coefficients with 95% confidence bounds are shown in Table 2. A straight line fit is found to be satisfactory as the goodness the fit (R^2) is close to one in all cases. Therefore, by knowing the vehicle speed it is possible to determine the CDR using the proposed calibration procedure, but it is hard to determine the location of the crack for low CDR.

Figure 9 shows a generic fit of damage calibration curve using the detection measures, i.e the calibration of standard deviation in the function of CDR for three different vehicle speeds (40; 80 and 130km/h representing low, medium and high vehicle speed

respectively), analysed separately for three different positions of the crack. The best fit is represented by power law equations. The relevant coefficients and indicators of goodnes of the fit are given in Table 3. A comprehensive numerical study based on the damage extent calibration using the proposed markers are provided as additional material along with this paper and is made available online. The markers are calibrated against CDR and the speed of the traversing vehicle.

6. Conclusions

This paper directly uses bridge deck surface roughness for damage detection in bridges through consideration of bridge-vehicle interaction effects. A new methodology in presented in this regard. Statistical descriptors are computed on a modified time domain response measure for consistent detection of the location and calibration of damage extent. It is shown that mean and standard deviation are consistent and monotonic descriptors of the system characteristics sensitive to crack presence. The first and second order cumulants of response can be efficiently used as damage detection markers, where discontinuity in the slope of the mean and standard deviation curves give the position of damage, with the jump size related to the extent of damage. The proposed methodology eliminates the need for complex analysis and can accommodate experimental observations and real time implementation easily. The fact that the proposed method is well-suited for output-only operational conditions has disadvantages and advantages. The disadvantage is that numerous sensors for monitoring structure operational conditions are needed, while the advantage is that the online monitoring of the structure is possible just by analysis of its response which can contribute to the SHM

of bridge structures to a significant extent. The consistency of calibration depends on the vehicle speed and road type. This is more pronounced in the case of higher damage. Damage calibration on better roads is less uncertain and gives consistent but less sensitive results. Worse roads are less consistent in calibration values but give more sensitive results. The study is particularly useful for continuous online bridge health monitoring since the data necessary for analysis can be obtained from the operating condition of the bridge and the structure does not therefore need be closed down.

Acknowledgements

The authors wish to thank the Irish Research Council (IRC) for providing grant to support this research.

References

1. O'Connor, A. and Eichinger, E. M., 2007, “Site-Specific Traffic Load Modelling for Bridge Assessment”, ICE Journal of Bridge Engineering., 160 (4), pp.185-194.

2. O'Connor, A. and Enevoldsen, I., 2009, “Probability-Based Assessment of Highway Bridges According to the New Danish Guideline”, Structure & Infrastructure Engineering: Maintenance, Management, Life-Cycl, 5 (2), pp.157-168.

3. O’Brien, E., Znidaric, A., Brady, K., Gonzalez, A. and O'Connor, A., 2005, “Procedures for the Assessment of Highway Structures”, ICE Transport Journal, 158 (TR1), pp.17-25.

4. Delgado, R. M. and dos Santos, R. C. S. M., 1997, “Modelling of a Railway Bridge–Vehicle Interaction on High Speed Tracks”, Computers and Structures, 63 (3), pp.511-523

5. Pesterev, A. V. and Bergman, L. A., 1997, “Vibration of Elastic Continuum Carrying Accelerating Oscillator”, ASCE Journal of Engineering Mechanics, 123 (8), pp.886-889.

6. Song, M.-K., Noh, H.-C. and Choi, C.-K., 2003, “A New Three-Dimensional Finite Element Analysis Model of High-Speed Train–Bridge Interactions”, Engineering Structures, 25 (13), pp.1611-1626.

7. Gentile, A. and Messina, A., 2003, “On the Continuous Wavelet Transforms Applied to Discrete Vibrational Data for Detecting Open Cracks in Damaged Beams”, International Journal of Solids and Structures, 40 (2), pp.295–315.

8. Patsias, S. and Staszewskiy, W. J., 2002, “Damage Detection Using Optical Measurements and Wavelets”, Structural Health Monitoring, 1 (1), pp.5-22.

9. Pakrashi, V., Basu, B. and Connor, A. O., 2009, “A Statistical Measure for Wavelet Based Singularity Detection”, Journal of Vibration and Acoustics, 131 (4), pp.041015 (6 pages)

10. Doebling, S. W., Farrar, C. R., Prime, M. B. and Shevitz, D. W., 1996, “Damage Identification and Health Monitoring of Structural and Mechanical Systems from Changes in Their Vibration Characteristics: A Literature Review”, Report No LA-13070-MS, Los Alamos National Laboratory is operated by the University of California for the United States Department of Energy under contract W-7405-ENG-36,

11. Narkis, Y., 1994, “Identification of Crack Location in Vibrating Simply Supported Beams”, Journal of sound and Vibrations, 172 (4), pp.Pages 549-558

12. Law, S. S. and Zhu, X. Q., 2004, “Dynamic Behaviour of Damaged Concrete Bridge Structures under Moving Vehicular Loads”, Engineering Structures, 26 (9), pp.1279–1293.

13. Majumder, L. and Manohar, C. S., 2003, “A Time Domain Approach for Damage Detection in Beam Structures Using Vibration Data with a Moving Oscillator as an Excitation Source. ”, Journal of Sound and Vibration, 268 pp. 699–716.

14. Lee, J. W., Kim, J. D., Yun, C. B., Yi, J. H. and Shim, J. M., 2002, “Health Monitoring Method for Bridges under Ordinary Traffic Loadings”, Journal of Sound and Vibration, 257 (2), pp.247–264.

15. Bilello, C., Bergman, A. L. and Kuchma, D., 2004, “Experimental Investigation of a Small-Scale Bridge Model under a Moving Mass”, ASCE Journal of Structural Engineering, 130 (5), pp.799–804.

16. Bilello, C. and Bergman, L. A., 2004, “Vibration of Damaged Beams under a Moving Mass: Theory and Experimental Validation”, Journal of Sound and Vibration, 274 (3-5), pp.567–582.

17. Pakrashi, V., O'Connor, A. and Basu, B., 2010, “A Bridge–Vehicle Interaction Based Experimental Investigation of Damage Evolution”, Structural Health Monitoring, 9 (4), pp.285 - 296.

18. Bu, J. Q., Law, S. S. and Zhu, X. Q., 2006, “Innovative Bridge Condition Assessment from Dynamic Response of a Passing Vehicle”, ASCE Journal of Engineering Mechanics, 132 (12), pp.1372–1379.

19. Abdel-Rohman, M. and Al-Duaij, J., 1996, “Dynamic Response of Hinged-Hinged Single Span Bridges with Uneven Deck”, Computers & Structures, 59 (2), pp.291-299.

20. da Silva, J. G. S., 2004, “Dynamical Performance of Highway Bridge Decks with Irregular Pavement Surface”, Computers & Structures, 82 (11-12), pp.871-881

21. Wu, S. Q. and Law, S. S., 2011, “Vehicle Axle Load Identification on Bridge Deck with Irregular Road Surface Profile”, Engineering Structures, 33 (2), pp.591-601

22. Sohn, H., Farrar, C. R., Hunter, N. F. and Worden, K., 2001, “Structural Health Monitoring Using Statistical Pattern Recognition Techniques”, ASME Journal of Dynamic Systems, Measurement and Control 123 (4), pp.706-717.

23. Cacciola, P., Impollonia, N. and Muscolino, G., 2003, “Crack Detection and Location in a Damaged Beam Vibrating under White Noise”, Computers and Structures, 81 pp.1773–1782.

24. Hadjileontiadis, L. J., Douka, E. and Trochidis, A., 2005, “Crack Detection in Beams Using Kurtosis”, Computers & Structures, 83 (12–13), pp.909-919.

25. Jaksic, V., Pakrashi, V. and O'Connor, A., 2011, “Employing Surface Roughness for Bridge-Vehicle Interaction Based Damage Detection”, ASME 2011 International Mechanical Engineering Congress and Exposition (IMECE 2011) Denver, Colorado, USA,

26. Jaksic, V. and Pakrashi, V., 2013, “Robust Skewness-Kurtosis Descriptor for Damping Calibration from Frequency Response”, Journal of Aerospace Engineering, 26 (4), pp. 887–893.

27. ISO 8606:1995(E). Mechanical vibration - road surface profiles-reporting of measured data.

28. Poudel, U. P., Fu, G. and Ye, J., 2005, “Structural Damage Detection Using Digital Video Imaging Technique and Wavelet Transformation”, Journal of Sound and Vibration, 286 (4-5), pp.869–895.

29. Sundermeyer, J. N. and Weaver, R. L., 1994, “On Crack Identification and Characterization in a Beam by Non-Linear Vibration Analysis”, Journal of Sound and Vibration, 183 (5), pp.857-871.

30. Henchi, K., Fafard, M., Talbot, M. and Dhatt, G., 1998, “An Efficient Algorthm for Dynamic Analysis of Bridges under Moving Vehicles Using a Coupled Modal and Physical Components Aproach”, Journal of Sound and Vibration, 212 (4), pp.663-683

31. Law, S. S. and Zhu, X. Q., 2005, “Bridge Dynamic Responses Due to Road Surface Roughness and Braking of Vehicle”, Journal of Sound and Vibration, 282 (3-5), pp.805-830

32. 2004. The MathWorks, Inc., Natick, Massachusetts.

33. Law, S. S., Bub, J. Q., Zhua, X. Q. and Chana, S. L., 2004, “Vehicle Axle Loads Identification Using Finite Element Method”, Engineering Structures, 26 (8), pp.1143-1153

34. Shen, M.-H. H. and Pierre, C., 1990, “Natural Modes of Bernoulli-Euler Beams with Symmetric Cracks”, Journal of Sound and Vibration 138 (1), pp.115-134.

35. Chang, C.-C. and Chen, L.-W., 2003, “Vibration Damage Detection of a Timoshenko Beam by Spatial Wavelet Based Approach ”, Applied Acoustics, 64 (12), pp.1217-1240

36. Okafor, A. C. and Dutta, A., 2000, “Structural Damage Detection in Beams by Wavelet Transforms”, Smart Materials and Structures, 9 (6), pp.906–917.

37. Loutridis, S., Doukab, E. and Trochidis, A., 2004, “Crack Identification in Double-Cracked Beams Using Wavelet Analysis ”, Journal of Sound and Vibration, 277 (4-5), pp.1025-1039

38. Qian, B. and Rasheed, K., 2004, “Hurst Exponent and Financial Market Predictability”, IASTED conference on Financial Engineering and Applications (FEA 2004), Cambridge, Massachusetts, USA, pp. 203 – 209.

39. Morales, R., Di Matteo, T., Gramatica, R. and Aste, T., 2012, “Dynamical Generalized Hurst Exponent as a Tool to Monitor Unstable Periods in Financial Time Series”, Physica A: Statistical Mechanics and its Applications, 391 (11), pp.3180-3189.

40. Vela-Martínez, L., Jáuregui-Correa, J. C. and Álvarez-Ramírez, J., 2009, “Characterization of Machining Chattering Dynamics: An R/S Scaling Analysis Approach”, International Journal of Machine Tools and Manufacture, 49 (11), pp.832-842.

41. Pakrashi, V., Kelly, J., Harkin, J. and Farrell, A., 2013, “Hurst Exponent Footprints from Activities on a Large Structural System”, Physica A: Statistical Mechanics and its Applications, 392 (8), pp.1803-1817.

List of Tables

Table 1

Road class	A Very good	B Good	C Average	D Poor	E Very poor
Roughness coefficient $S_d(f_0)$ (m^3/cycle) × 10^{-6}	6	16	64	256	1024

Table 2

General form of fit is linear polynomial equation $\sigma = a \times V_V + b$

X_c / CDR	0.1L	0.25L	0.5L
0.10	a = -1.209e-007 b = 2.567e-006 SSE: 2.209e-013 R^2 = 0.9378	a = -2.224e-007 b = 4.795e-006 SSE: 9.34e-013 R^2 = 0.9234	a = -1.062e-007 b = 2.233e-006 SSE: 1.747e-013 R^2 = 0.9362
0.25	a = -7.436e-007 b = 1.553e-005 SSE: 7.513e-012 R^2 = 0.9436	a = -1.368e-006 b = 2.842e-005 SSE: 2.514e-011 R^2 = 0.9443	a = -6.743e-007 b = 1.418e-005 SSE: 5.505e-012 R^2 = 0.9495
0.40	a = -2.199e-006 b= 4.401e-005 SSE: 5.689e-011 R^2 = 0.9508	a = -3.823e-006 b = 7.512e-005 SSE: 2.346e-010 R^2 = 0.9341	a = -2.321e-006 b = 4.624e-005 SSE: 8.783e-011 R^2 = 0.9331

Table 3

General form of fit is power equation $\sigma = a \times CDR^b + c$

V_V \ X_c	0.1L	0.25L	0.5L
low	a = 0.0001925 b = 1.997 c = -4.744e-007 SSE: 2.266e-012 R^2 = 0.9981	a = 0.0002747 b = 1.916 c = 4.194e-007 SSE: 2.816e-012 R^2 = 0.999	a = 0.0002072 b = 2.022 c = -1.595e-006 SSE: 1.211e-011 R^2 = 0.9912
medium	a = 0.0001756 b = 1.986 c = -7.936e-007 SSE: 2.648e-012 R^2 = 0.9974	a = 0.0002629 b = 1.935 c = 6.323e-007 SSE: 2.954e-012 R^2 = 0.9988	a = 0.0002058 b = 2.091 c = -1.478e-006 SSE: 1.109e-011 R^2 = 0.991
high	a = 8.9e-005 b = 1.899 c = -6.129e-007 SSE: 8.243e-013 R^2 = 0.9973	a = 0.0001353 b = 1.88 c = -7.43e-008 SSE: 8.575e-014 R^2 = 0.9999	a = 0.0001084 b = 2.053 c = -8.127e-007 SSE: 2.524e-012 R^2 = 0.993

List of Figures

Figure 6. a) Mean (μ) and; b) Standard Deviation (STD) variation in function of Crack Depth Ratio (CDR) for different position of crack location (Xc) and; c) Mean; and d) STD in function of Xc for different CDR; while speed of vehicle is constant and type of road is class C as per ISO 8606:1995(E).

Figure 7. Mean (μ) and Standard Deviation (STD) variation in function of Crack Depth Ratio (CDR) for different Road Type defined as per ISO 8606:1995(E) analyzed for three different Vehicle speed (Vv): Low, Medium and High.

Figure 8. Calibration of Standard Deviation (STD) variation in function Vehicle speed (Vv): Low, Medium and High; for three different positions of the damage: a) Edge; b) Quarter-span and c) Mid-span.

Figure 9. Calibration of Standard Deviation (STD) variation in function Crack Depth Ratio (CDR); for Low, Medium and High Vehicle Speed (Vv) and three different positions of the damage: a) Edge; b) Quarter-span and c) Mid-span.

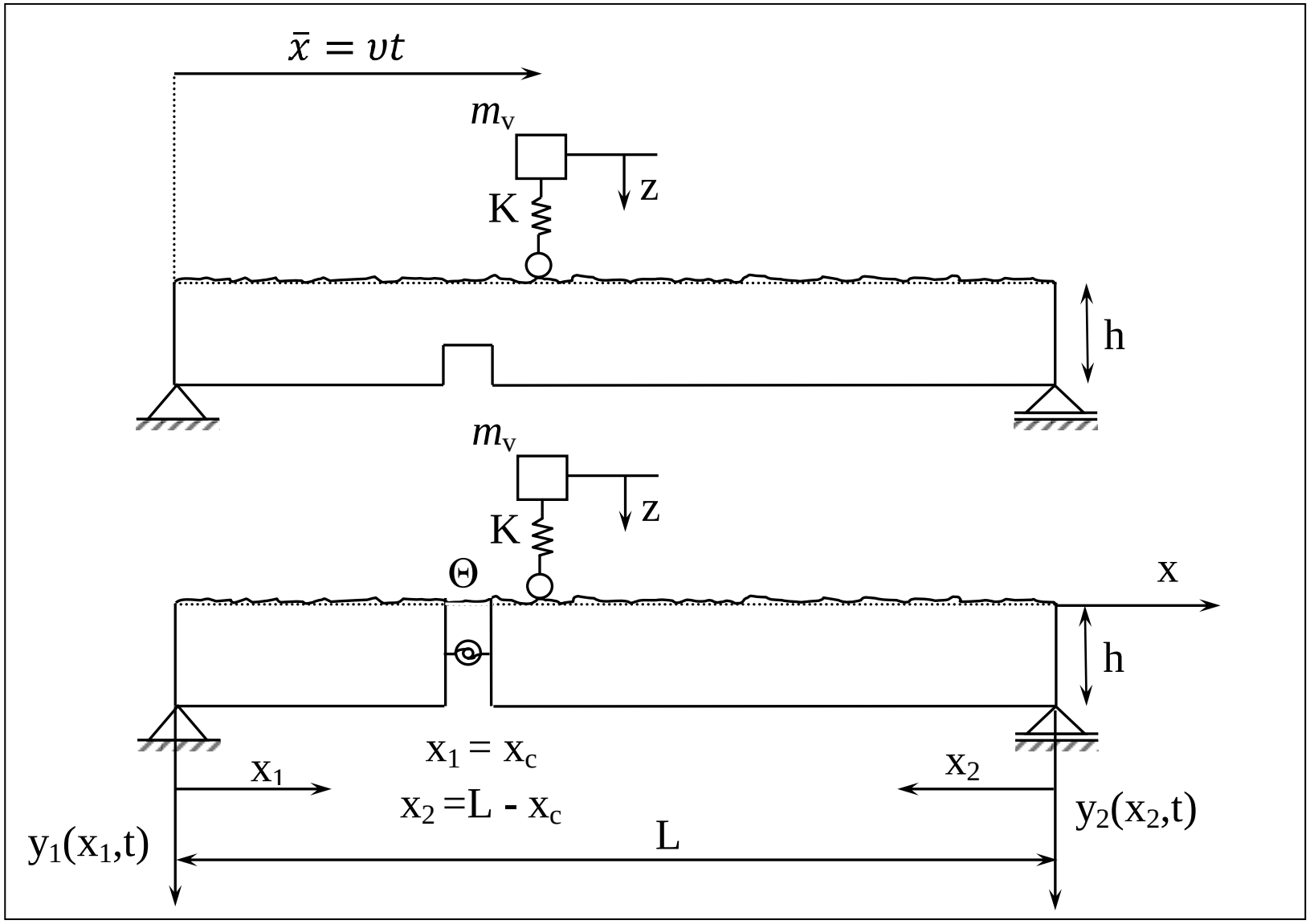

Figure 1.

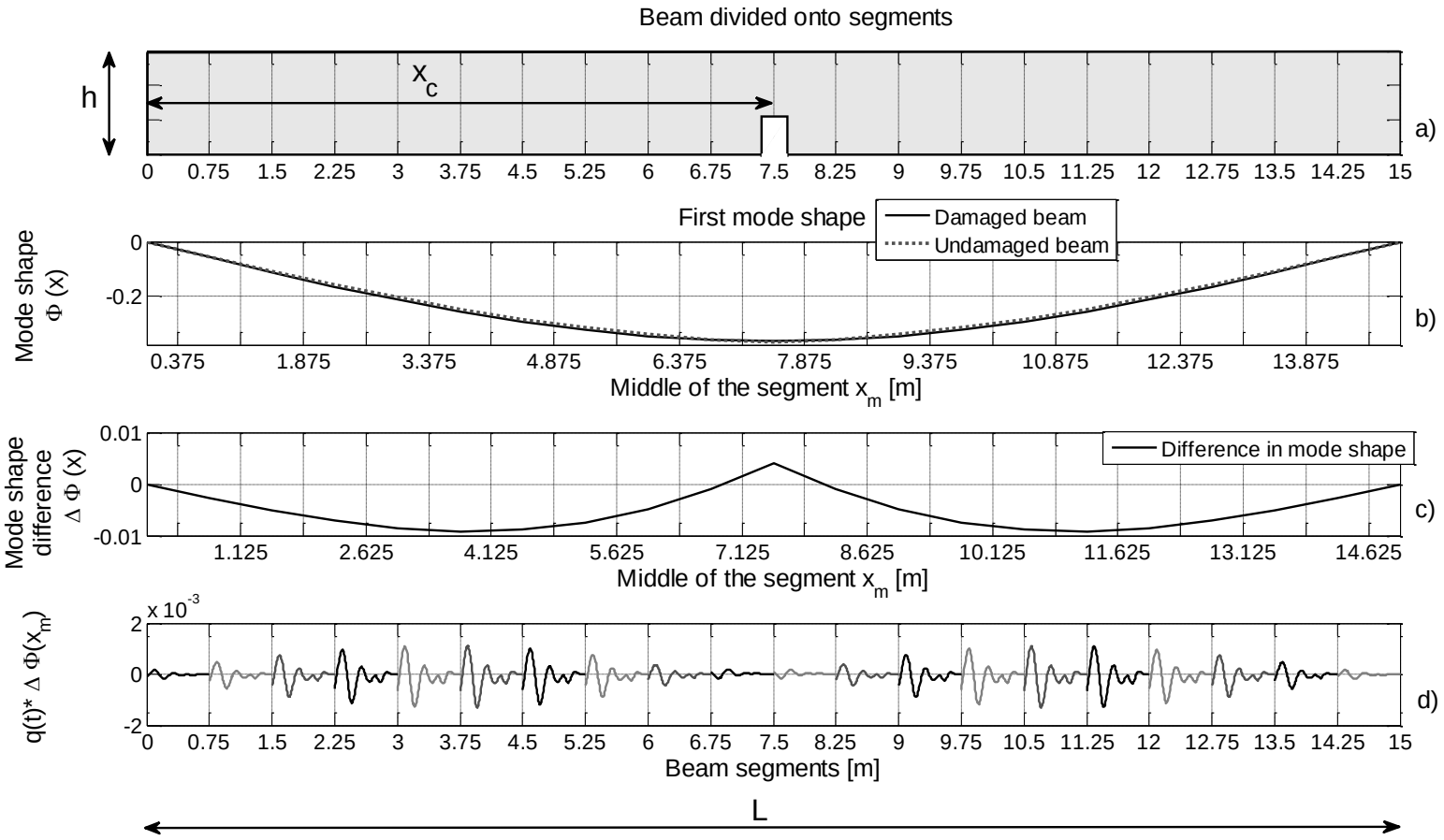
Beam divided onto segments
h
x_c
a)
0 0.75 1.5 2.25 3 3.75 4.5 5.25 6 6.75 7.5 8.25 9 9.75 10.5 11.25 12 12.75 13.5 14.25 15
First mode shape
Damaged beam
Undamaged beam
Mode shape Φ (x)
0
-0.2
b)
0.375 1.875 3.375 4.875 6.375 7.875 9.375 10.875 12.375 13.875
Middle of the segment x_m [m]
Mode shape difference Δ Φ (x)
Difference in mode shape
0.01
0
-0.01
c)
1.125 2.625 4.125 5.625 7.125 8.625 10.125 11.625 13.125 14.625
Middle of the segment x_m [m]
q(t)* Δ Φ(x_m)
x 10^{-3}
2
0
-2
d)
0 0.75 1.5 2.25 3 3.75 4.5 5.25 6 6.75 7.5 8.25 9 9.75 10.5 11.25 12 12.75 13.5 14.25 15
Beam segments [m]
L

Figure 2.

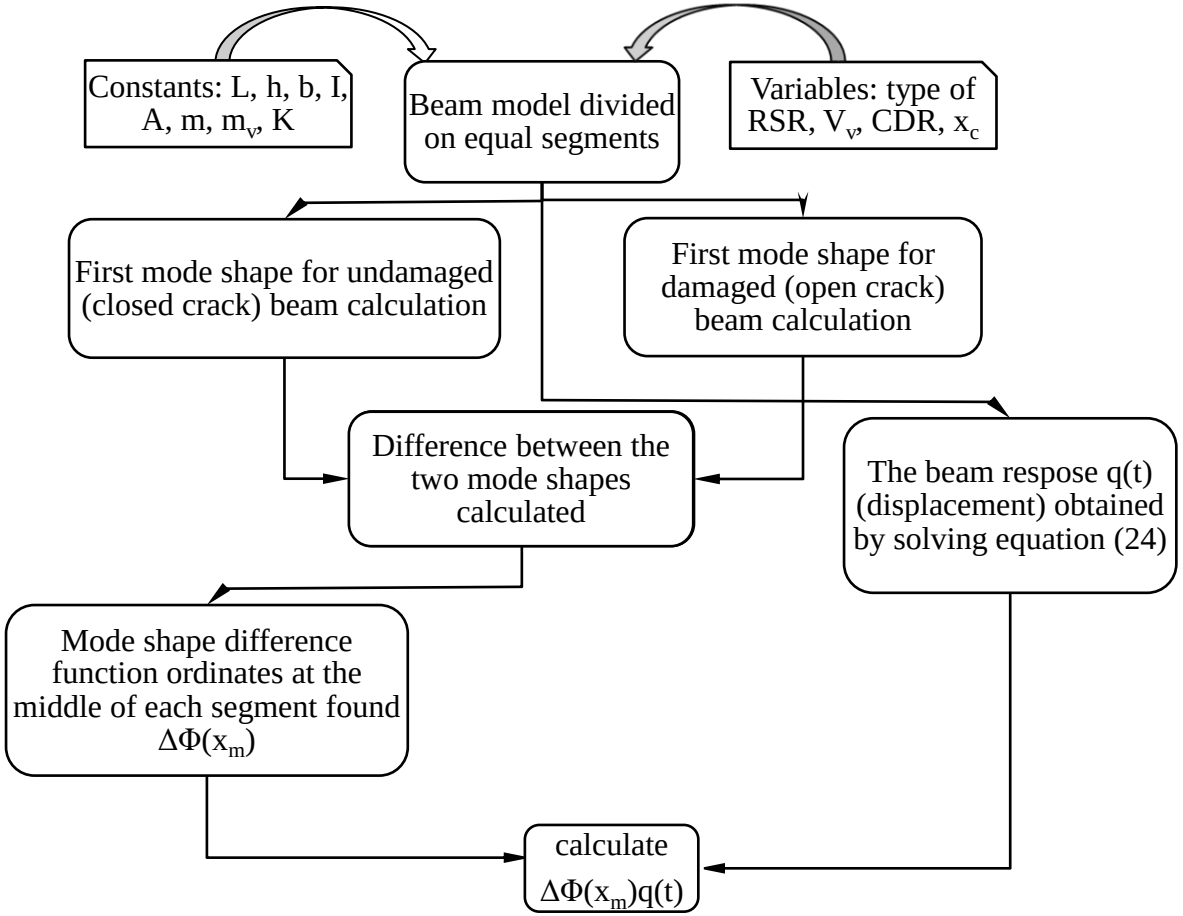
Constants: L, h, b, I, A, m, m_v, K
Beam model divided on equal segments
Variables: type of RSR, V_v, CDR, x_c
First mode shape for undamaged (closed crack) beam calculation
First mode shape for damaged (open crack) beam calculation
Difference between the two mode shapes calculated
The beam respose q(t) (displacement) obtained by solving equation (24)
Mode shape difference function ordinates at the middle of each segment found $\Delta\Phi(x_m)$
calculate $\Delta\Phi(x_m)q(t)$

Figure 3.

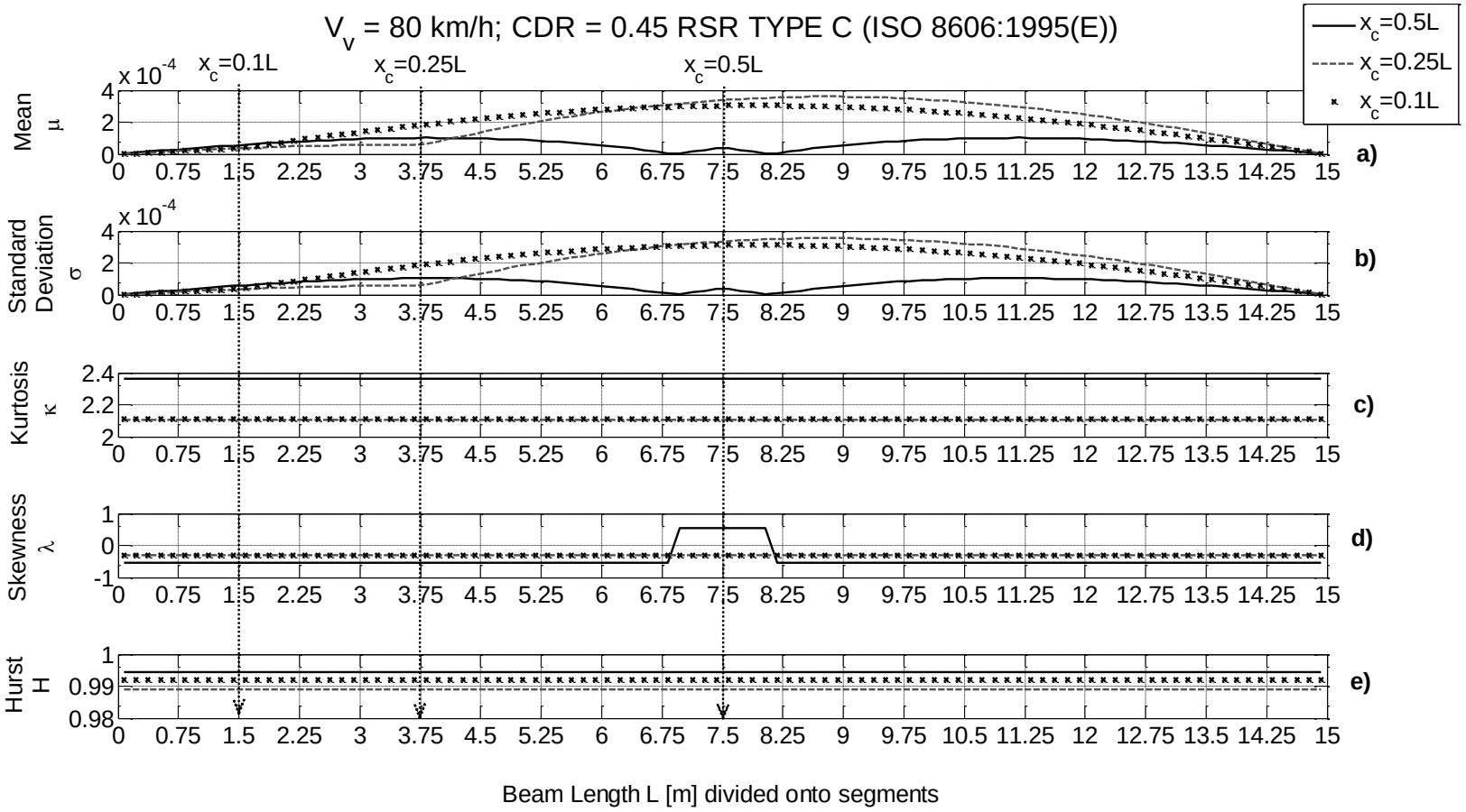
V_v = 80 km/h; CDR = 0.45 RSR TYPE C (ISO 8606:1995(E))
x_c=0.5L
x_c=0.25L
x_c=0.1L
x_c=0.1L
x_c=0.25L
x_c=0.5L
Mean μ
x 10^-4
Standard Deviation σ
x 10^-4
Kurtosis κ
Skewness λ
Hurst H
a)
b)
c)
d)
e)
0 0.75 1.5 2.25 3 3.75 4.5 5.25 6 6.75 7.5 8.25 9 9.75 10.5 11.25 12 12.75 13.5 14.25 15
Beam Length L [m] divided onto segments

Figure 4.

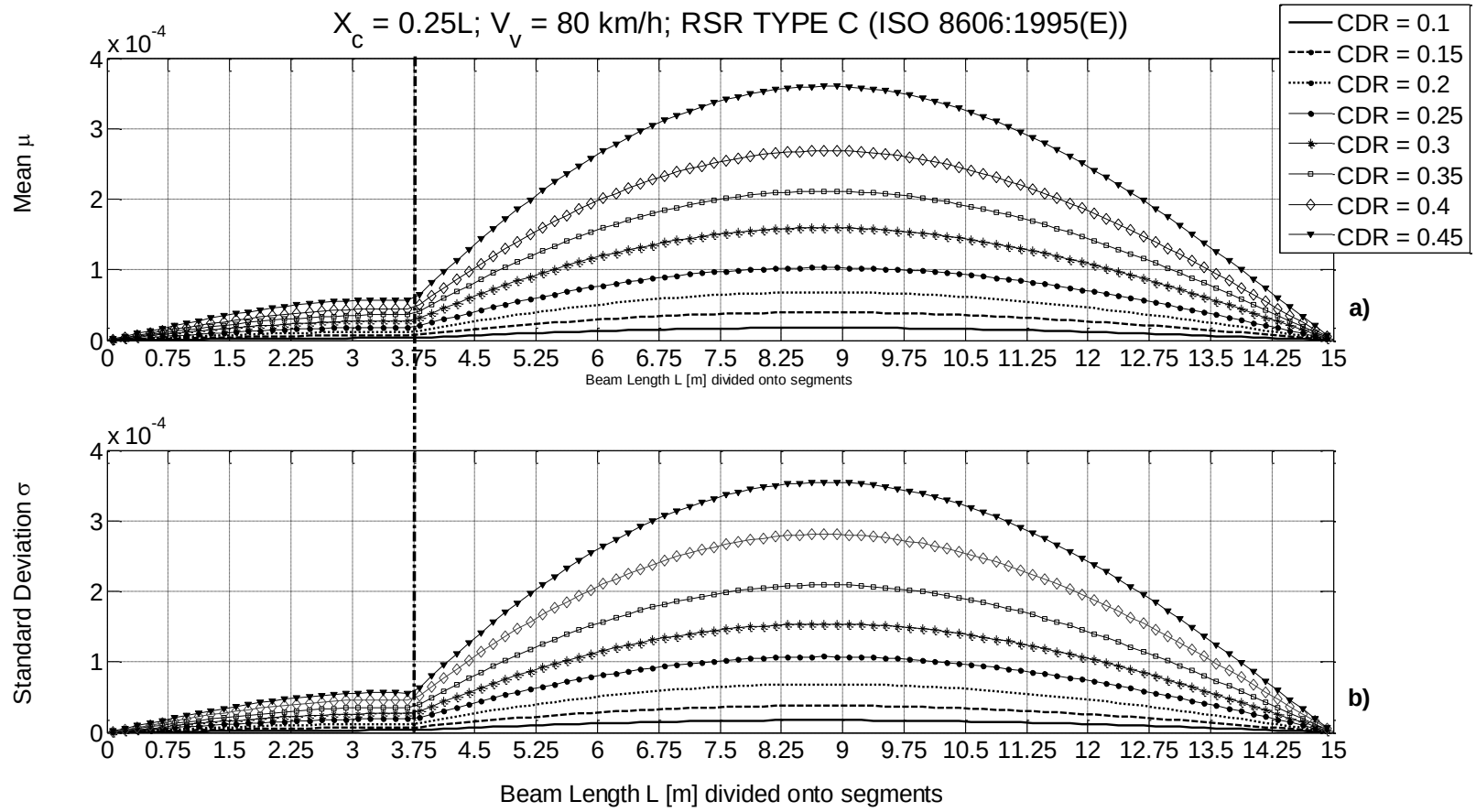
X_c = 0.25L; V_v = 80 km/h; RSR TYPE C (ISO 8606:1995(E))
CDR = 0.1
CDR = 0.15
CDR = 0.2
CDR = 0.25
CDR = 0.3
CDR = 0.35
CDR = 0.4
CDR = 0.45
Mean μ
x 10^-4
a)
Beam Length L [m] divided onto segments
Standard Deviation σ
x 10^-4
b)
Beam Length L [m] divided onto segments

Figure 5.

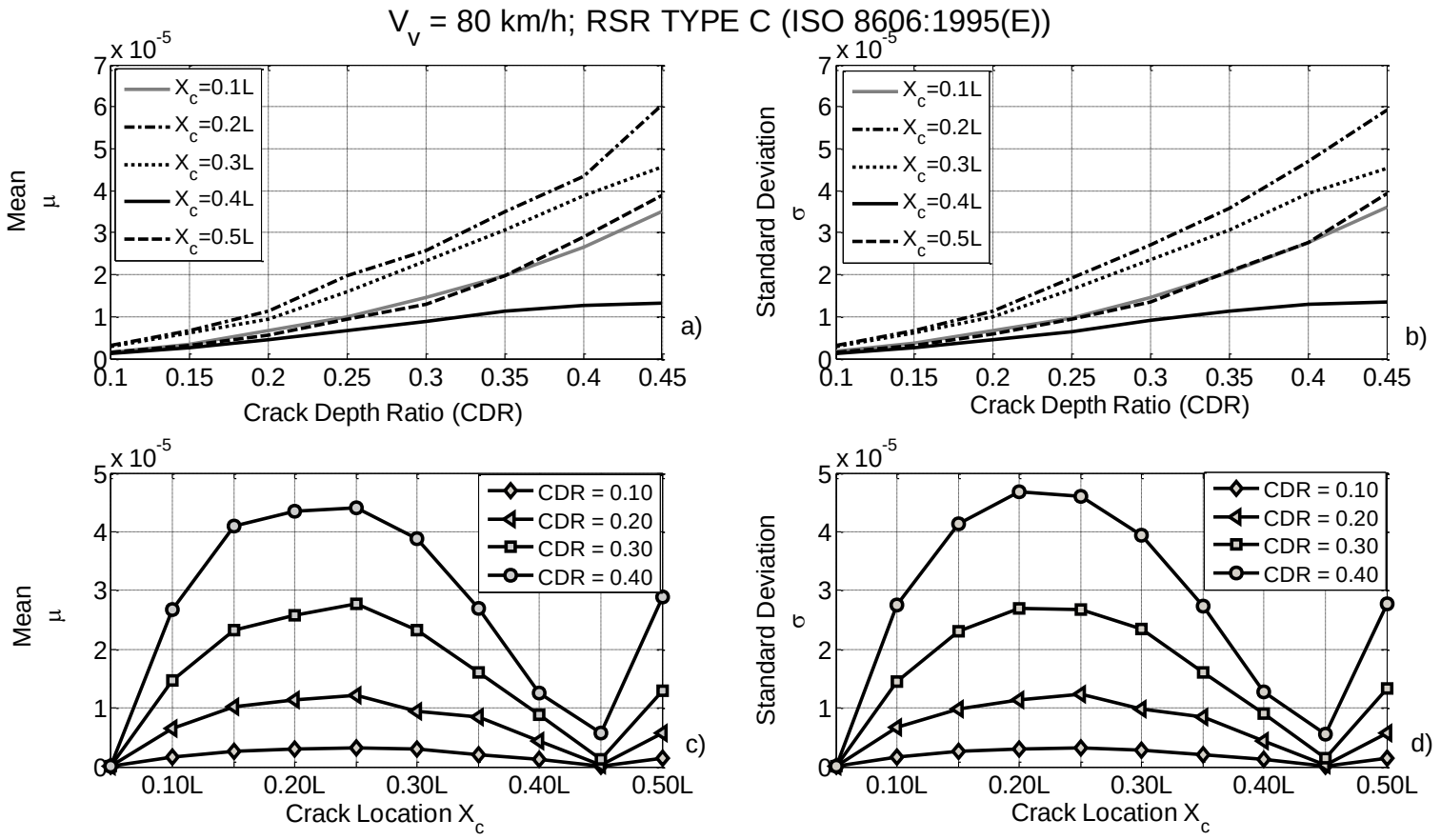
V_V = 80 km/h; RSR TYPE C (ISO 8606:1995(E))
x 10^-5
Mean μ
Standard Deviation σ
X_c=0.1L
X_c=0.2L
X_c=0.3L
X_c=0.4L
X_c=0.5L
Crack Depth Ratio (CDR)
a)
b)
CDR = 0.10
CDR = 0.20
CDR = 0.30
CDR = 0.40
0.10L
0.20L
0.30L
0.40L
0.50L
Crack Location X_c
c)
d)

Figure 6.

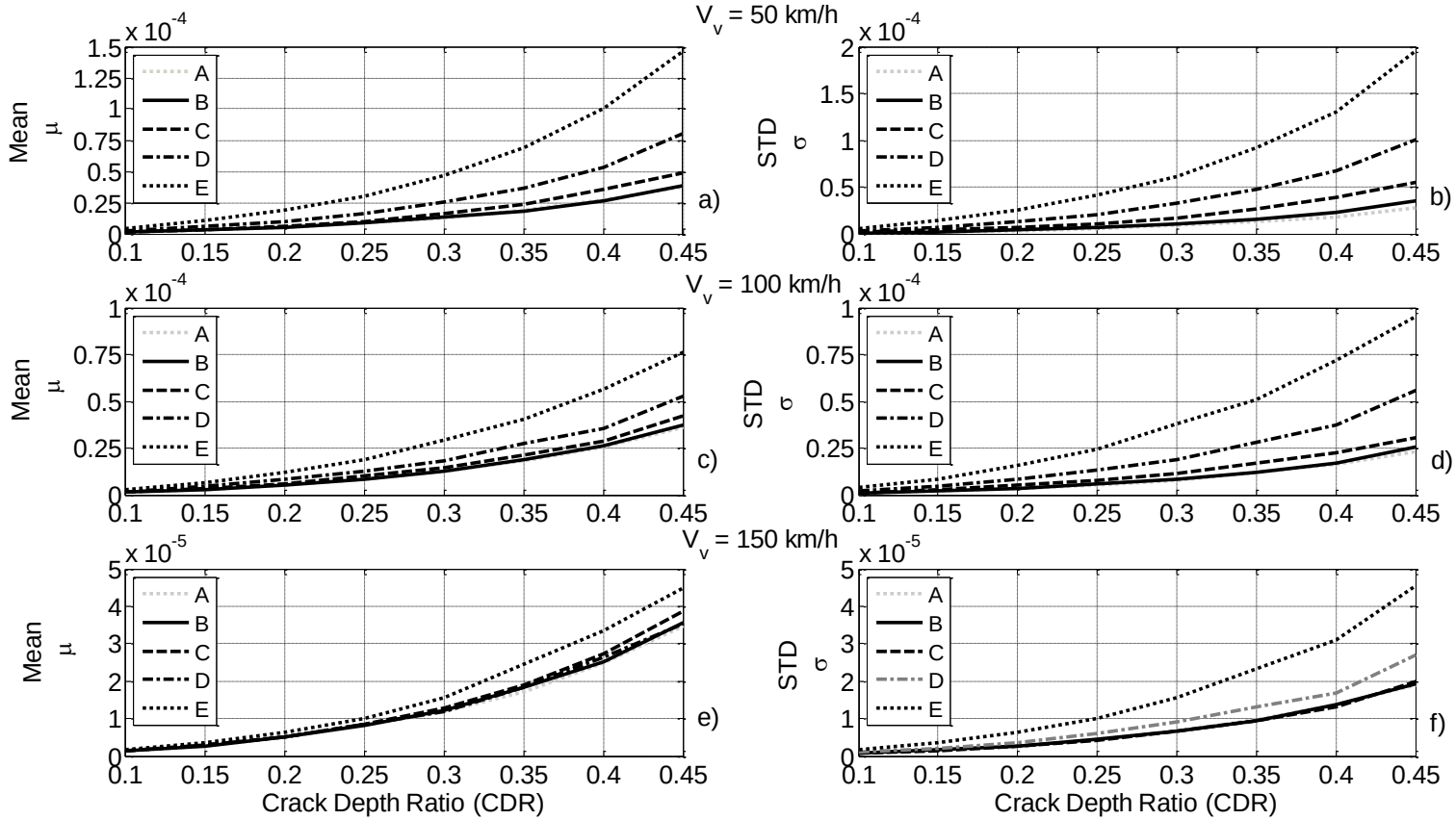
V_v = 50 km/h
V_v = 100 km/h
V_v = 150 km/h
Mean μ
STD σ
x 10^-4
x 10^-5
A
B
C
D
E
a)
b)
c)
d)
e)
f)
Crack Depth Ratio (CDR)
Crack Depth Ratio (CDR)

Figure 7.

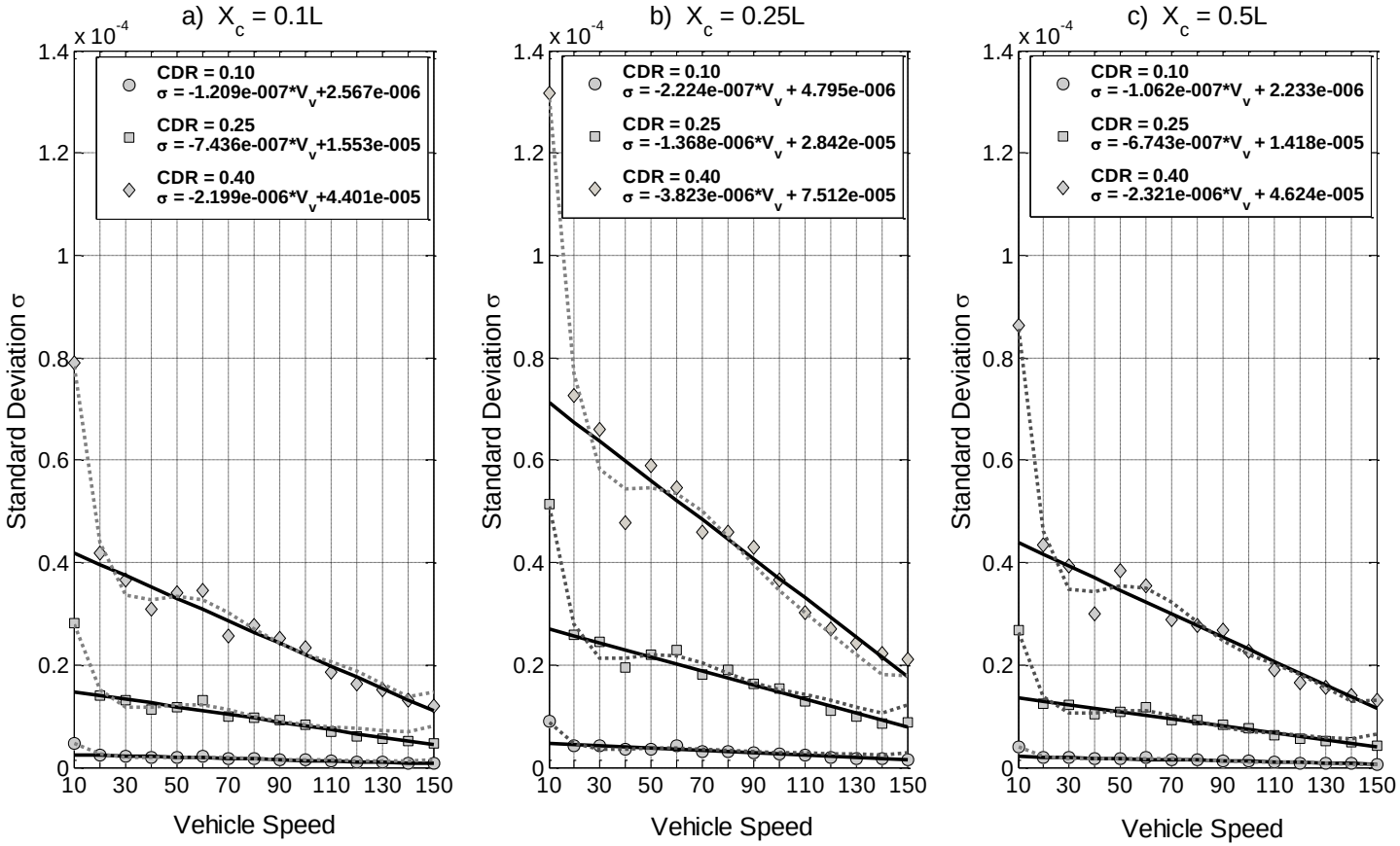
a) X_c = 0.1L
b) X_c = 0.25L
c) X_c = 0.5L
x 10^-4
Standard Deviation σ
Vehicle Speed
CDR = 0.10
σ = -1.209e-007*V_v+2.567e-006
CDR = 0.25
σ = -7.436e-007*V_v+1.553e-005
CDR = 0.40
σ = -2.199e-006*V_v+4.401e-005
CDR = 0.10
σ = -2.224e-007*V_v + 4.795e-006
CDR = 0.25
σ = -1.368e-006*V_v + 2.842e-005
CDR = 0.40
σ = -3.823e-006*V_v + 7.512e-005
CDR = 0.10
σ = -1.062e-007*V_v + 2.233e-006
CDR = 0.25
σ = -6.743e-007*V_v + 1.418e-005
CDR = 0.40
σ = -2.321e-006*V_v + 4.624e-005

Figure 8.

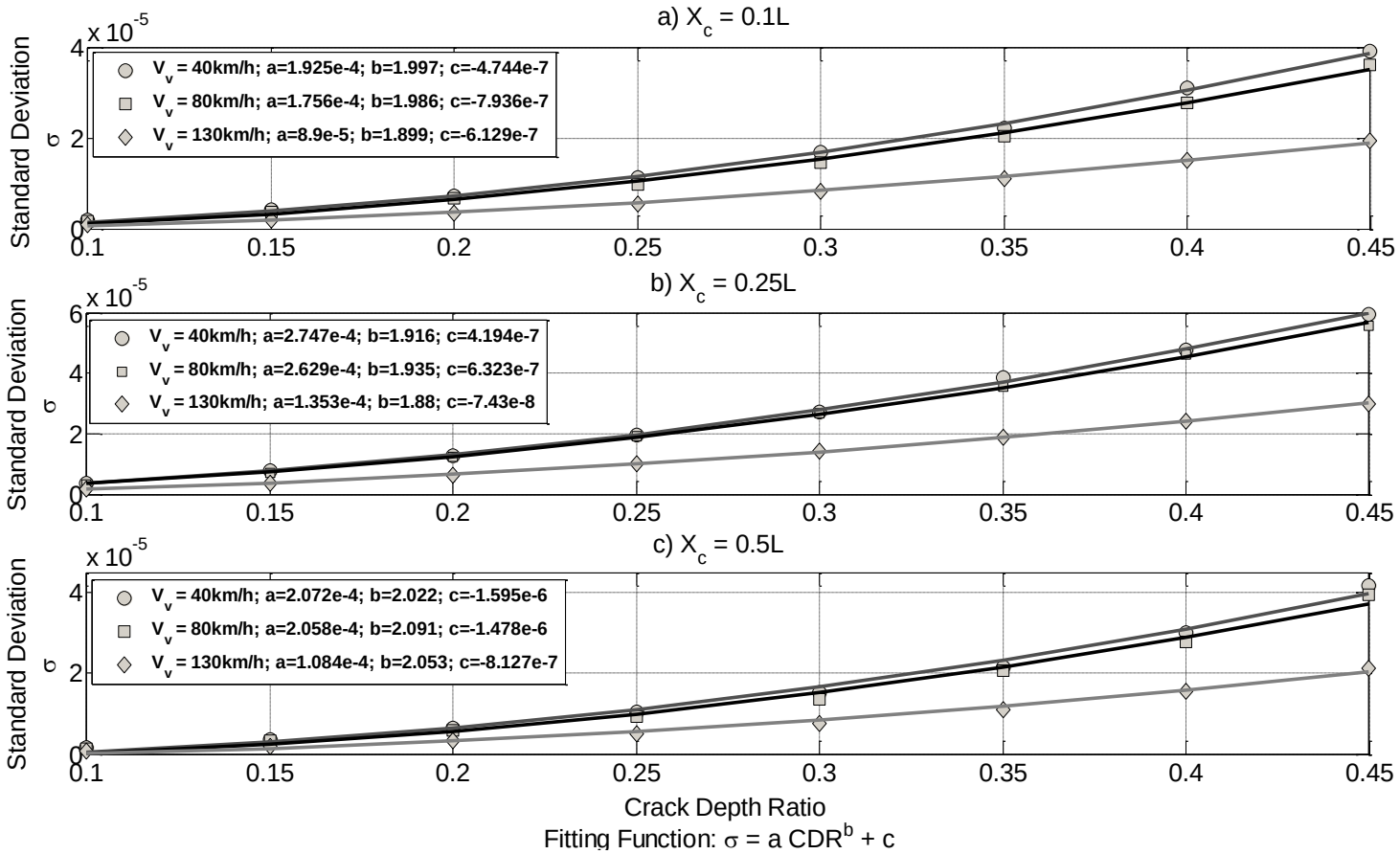
a) X_c = 0.1L
x 10^-5
Standard Deviation
σ
V_v = 40km/h; a=1.925e-4; b=1.997; c=-4.744e-7
V_v = 80km/h; a=1.756e-4; b=1.986; c=-7.936e-7
V_v = 130km/h; a=8.9e-5; b=1.899; c=-6.129e-7
b) X_c = 0.25L
V_v = 40km/h; a=2.747e-4; b=1.916; c=4.194e-7
V_v = 80km/h; a=2.629e-4; b=1.935; c=6.323e-7
V_v = 130km/h; a=1.353e-4; b=1.88; c=-7.43e-8
c) X_c = 0.5L
V_v = 40km/h; a=2.072e-4; b=2.022; c=-1.595e-6
V_v = 80km/h; a=2.058e-4; b=2.091; c=-1.478e-6
V_v = 130km/h; a=1.084e-4; b=2.053; c=-8.127e-7
0.1
0.15
0.2
0.25
0.3
0.35
0.4
0.45
Crack Depth Ratio
Fitting Function: σ = a CDR^b + c

Figure 9.